01NVSOQ – Advanced Antenna Engineering
Assignment 4: array components

Amedeo Bertone (243878)
Davide Botteon (239595)
Enrico Maria Renzi (244028)

January 18, 2018

Contents

1 Introduction

The goal of this project is the simulation of the complete structure realizing a four element array with amplitude tapering, obtaining a SLL of -20 dB.

The design is the same one we proposed in the previous assignment, but all the components will undergo a process of optimization in order to make us able to provide reliable and complete simulations finally attesting the correct behavior of the structure.

The first part will deal with the simulation and optimization of the power splitters that will later be inserted in the BFN. Both the even and uneven power splitter will be tested in order to identify the discontinuities present in the model and minimizing their effect.

The second part is related to the simulation of the BFN, in order to verify if the previously optimized splitters still work the right way when united in a single model and to correct the structure if not.

Last, in the third and final part, the complete antenna will be tested and its radiating properties will finally be verified, allowing us to finally understand if the BFN feeds the structure in a way that fulfills the design requirements or not.

At the end of the three described phases, a cad file will be produced containing the information about the final structure a producer would need in order to print the antenna.

2 Sections fine tuning

First T First of all we have to better optimize the various part of the beam forming network, and so we started considering the first T junction with the lines routing to the second one. In particular the bending situated between the T junction are introducing a strong discontinuity, which must be considered in the optimization. About the optimization of the bending and the use of the mitered solution for the T junction there are Appendix A and Appendix B that explains the process in details. Below we can see the results obtained in this way.

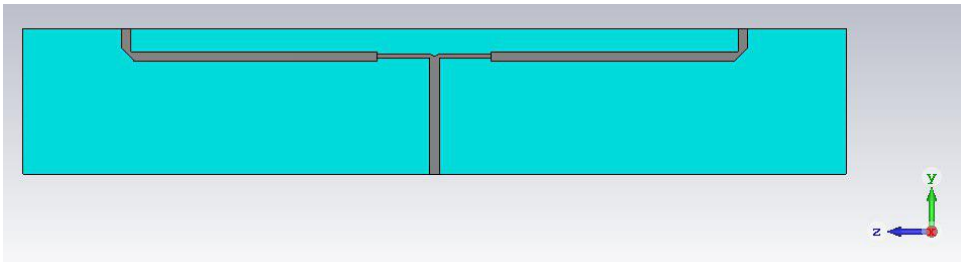

Figure 1: structure of the first T and the branches routing to the second one

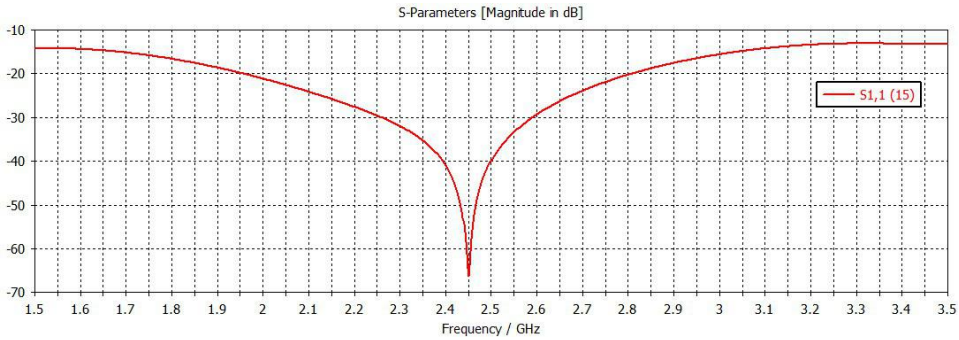

Figure 2: final scattering parameters

Second T Regarding the optimization of the second T junction we used the T designed for the previous assignment and we connect to it the two lines routing to the patches. In this way we control also the contributions due to the discontinuities on all the second part of the beam forming network.

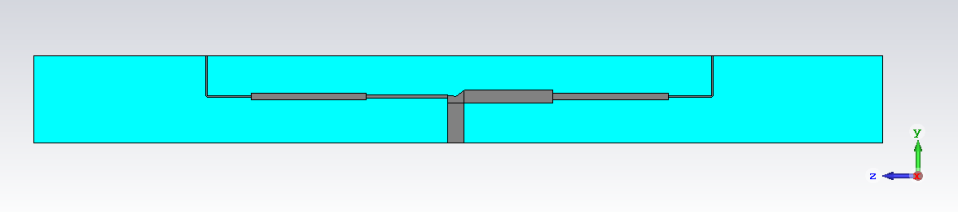

Figure 3: structure of the second T and the branches routing to the patches

Simulating this new component we have that the matching is no more on the wanted frequency of $2.45GHz$ but some megahertz higher. In order to make it decrease at first we tried to change the values external to the T junction with a freedom degree, that in particular are the angle and the tapering of the bending (the same process used for the first T, described above). The results varying those values are showed in the graphs below. Notice that in practice the resonance is not moved in both the cases.

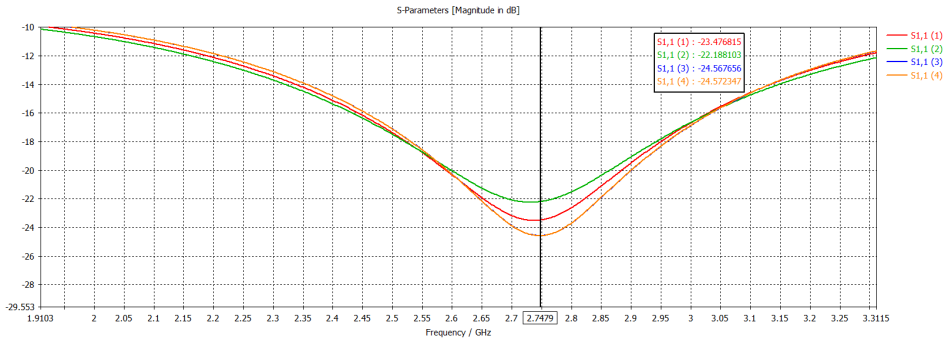

Figure 4: s11 with respect to the bend angle

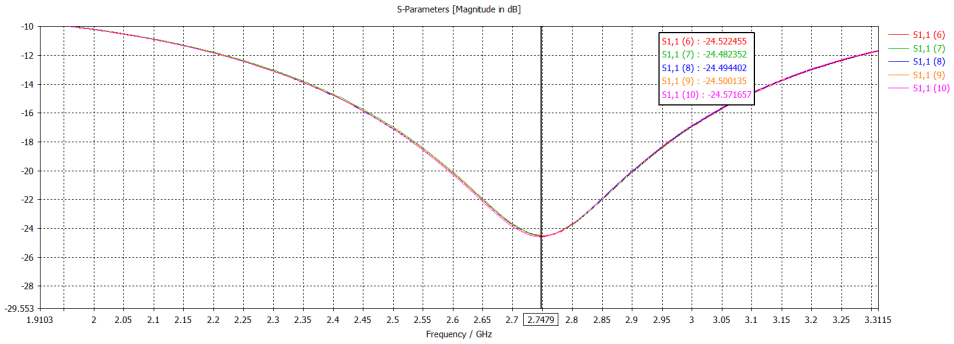

Figure 5: s11 with respect to the bend tapering

Now we have tried to not modify the T junction parameters, but since this way didn't produce the desired effect we have to change the the $\lambda/4$ impedance transformer's length (changing the other lines' length means changing the tapering). The graphs below shows the values obtained first with simply changing the transformer length and second the also re-using the old optimized value of the single T junction (notice that in the second case the return losses are lower).

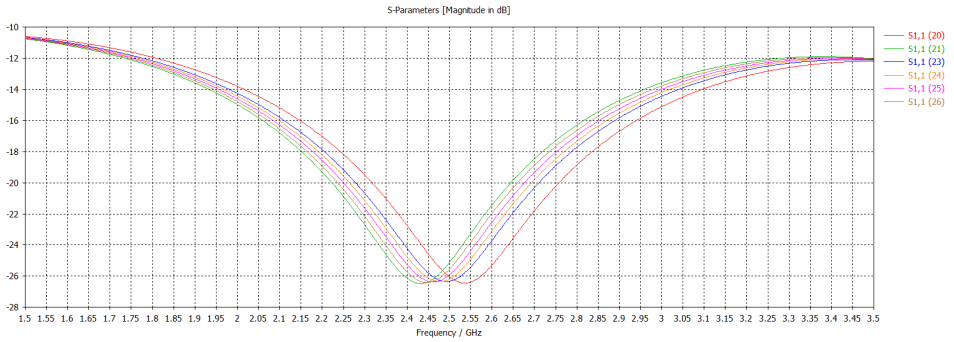

Figure 6: s11 with respect to the $\lambda/4$ transformer's length

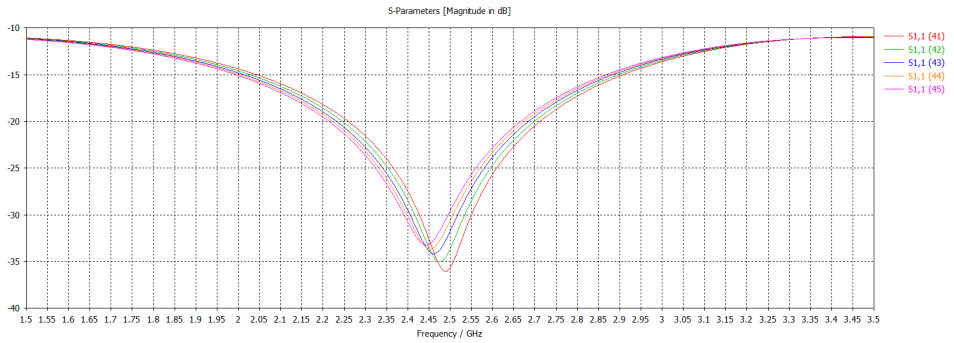

Figure 7: s11 with respect to the $\lambda/4$ transformer's length – changed values

With this final value we reached the desired behavior, so we can use this for composing the complete beam forming network. On the following figure is showed the result, notice that also the s_{21} and the s_{31} have the proper values in order to generate the desired tapering.

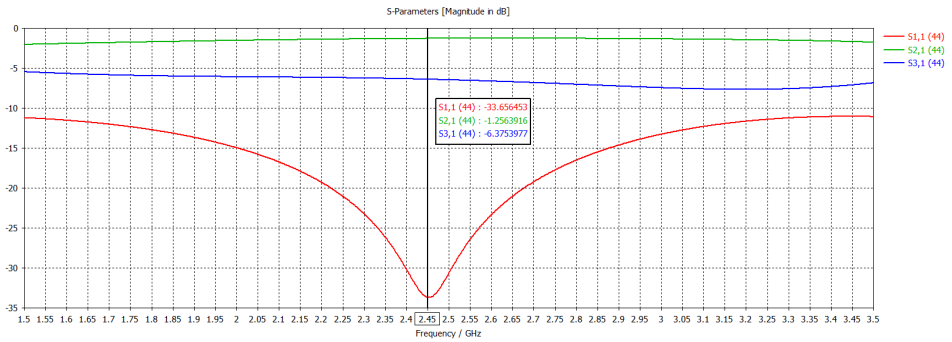

Figure 8: final scattering parameters

3 BFN fine tuning

Before proceeding with the simulation of the overall antenna we decided to perform an optimization of the BFN.

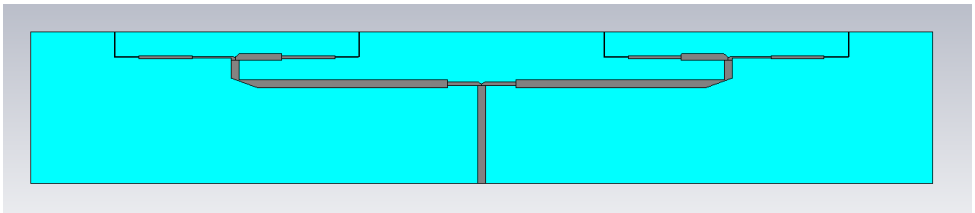

Figure 9: How the final BFN looks like

The attention was mainly focused on:

- tuning of the S_{11} parameter, in order to obtain a resonant behavior at 2.45 GHz
- achieving the best possible tapering, i.e. as close as possible to the theoretical value of 5.3 dB needed in order to get the right SLL in the final structure
- obtaining the right phasing between the elements, i.e. phase difference as close as possible to zero, since the array must be broadside.

Before showing the results of the simulations it is worth to spend a few words about meshes; in fact, as explained in class, the correct definition of the meshgrid is fundamental in order to assure the correct behavior of the waveguide ports and a reliable analysis of all the discontinuities present inside the model. That being said, we decided to impose a refinement of the grid across the more sensitive areas (thin elements and discontinuities) and second, a symmetry plane, which allowed to reduce the simulation time thanks to the intrinsic symmetry of the structure. Figure 10 gives an idea of how thin the mesh was around the critical points, while figures 11 and 12 show exactly how the settings were manipulated in order to obtain it.

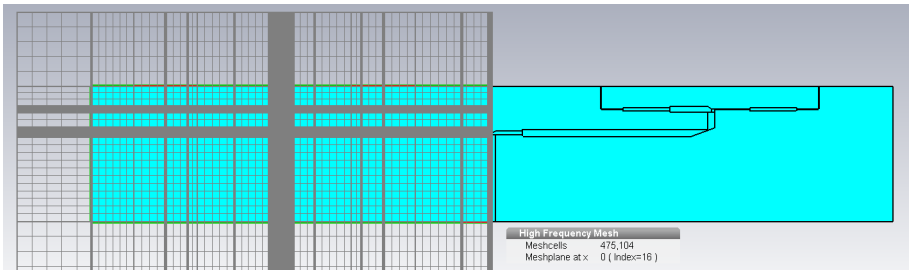

Figure 10: Mesh View of the BFN, showing the used symmetry plane setting too

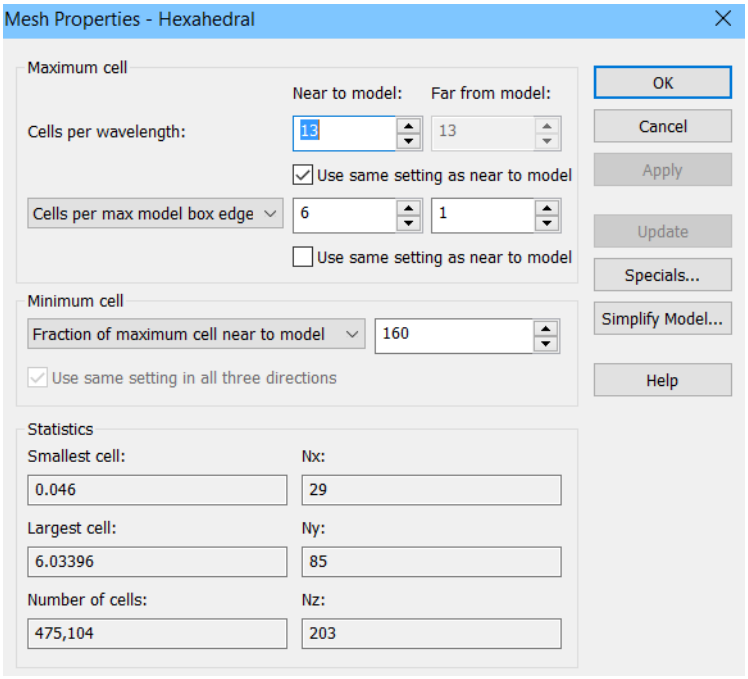

Figure 11: Imposed Mesh Properties

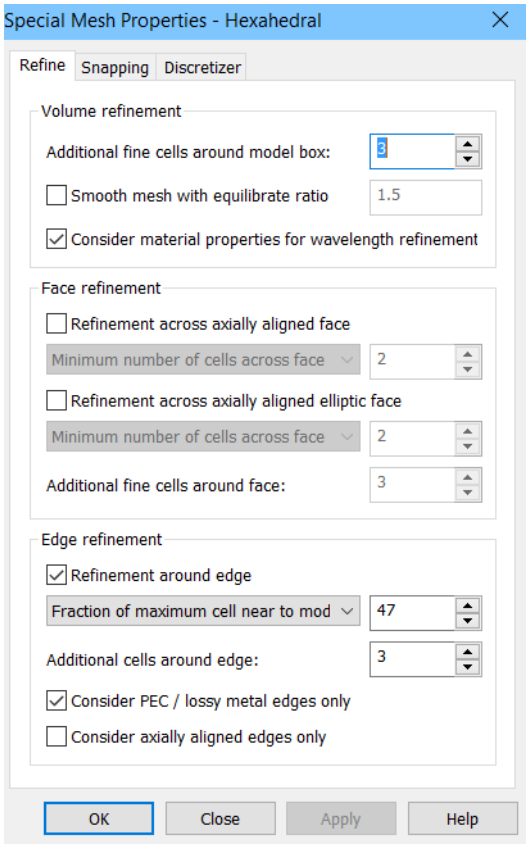

Figure 12: Imposed Special Mesh Properties

Now that we've concluded the discussion about adopted procedures (which obviously included a certain number of parametric sweeps and optimizer runs in order to refine the results) we can discuss the obtained parameters.

First, the S_{11} is shown, figure 13. The resonance point coincides almost exactly with 2.45 GHz and its level in dB is quite reassuring (-35 dB). It has to be said that we were able to obtain even lower values for our resonance (-45 dB), but in the end the shown solution was chosen because of its better behavior in terms of tapering and of the better results obtained when simulating it with the radiating elements.

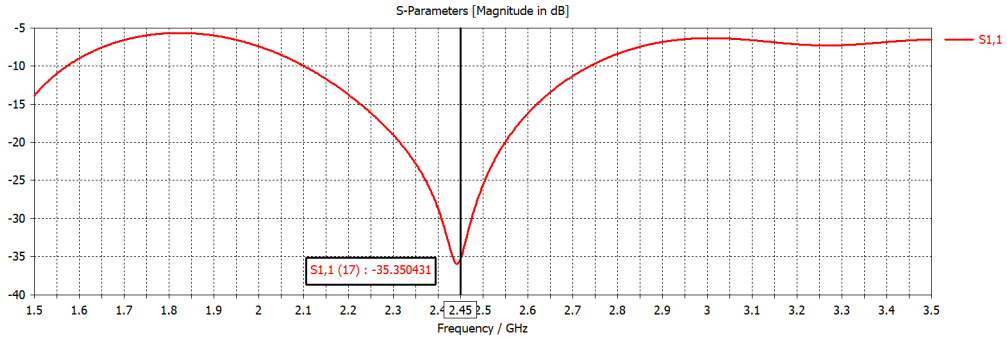

Figure 13: S_{11} parameter of our BFN

As figures 14 and 15 show, the tapering is around 5.05 dB while the phase difference between adjacent elements is lower than 1°.

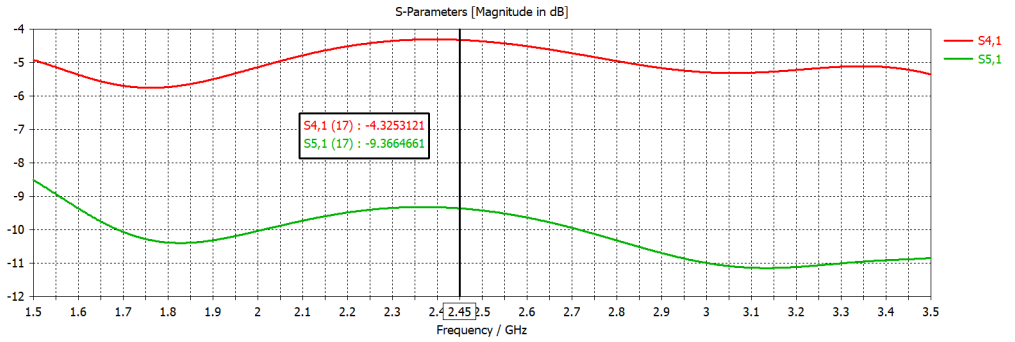

Figure 14: behavior in terms of tapering

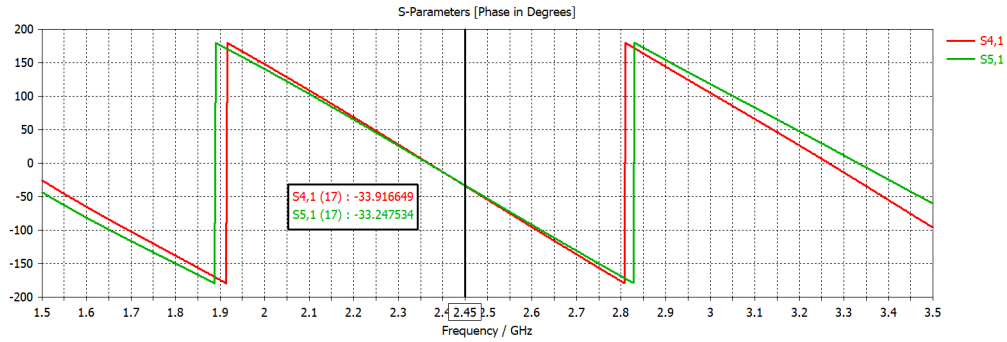

Figure 15: behavior in terms of phase

Last but not least, figure 16 shows an estimation of the -10 and -20 dB obtained bandwidths.

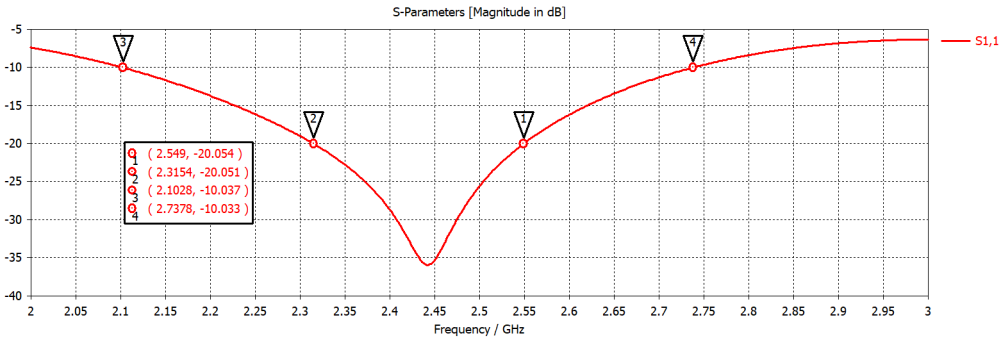

Figure 16: estimation of the bandwidth of the BFN

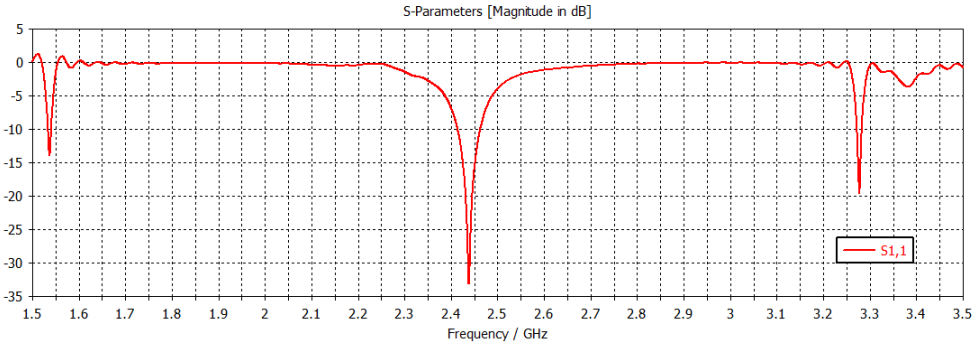

Figure 17: Broadband view for the input reflection coefficient seen from full array input port.

4 Full array fine tuning and results

Within this last step the tuned BFN and radiating part are connected. The spacing between elements is set to be compliant with the GL limit at the central resonance frequency f_0=2.45GHz (distance between elements, d=$\leq$88mm). Actually what follows mainly concerns the full antenna's radiation pattern, rather than the array factor alone. This is legitimated by the following facts:

- what can be measured to describe the real radiation properties of a microstrip array antenna is the far field radiation pattern;
- the full AF's extraction from simulation introduces numerical errors that makes the calculation inaccurate far from the main lobe centre.

Furthermore, moving the GL requirement from AF to the radiation patter, we gain a more robust design, less affected by discontinuities' and line width's losses[1].

Patch's width and length are set equal to: W_{patch}=64mm and L_{patch}=24.7mm. Once BFN and radiators have been joint, we have the complete array reported in figure 19, which has been simulated with the mesh settings printed in figure 20. To keep the computation simpler we exploited the microstrip field distribution and a (y,z) transverse magnetic field symmetry plane has been used as boundary condition (with open boundary, added space in all directions).

Finally, the simulation's outcomes are the following:

Return loss and bandwidth Overall, the input reflection coefficient is worsened by the connection of the two parts. Although the various

[1]the total radiation pattern is given by the product of the single patch's pattern and the normalized array factor. Since the former term damps the latter then the total radiated field will be lowered as well. Moreover we can relax the requirement on tapering having more uniform microstrip lines (in terms of width).

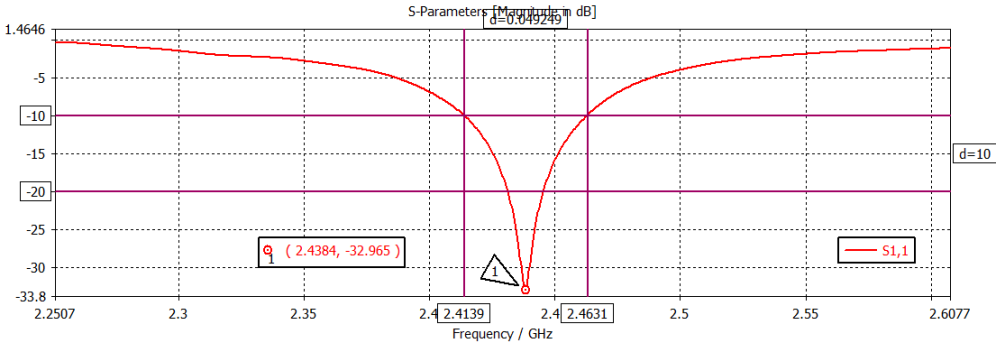

Figure 18: In-band view for the input reflection coefficient seen from full array input port.

sections have been finely tuned, the difference between using excitation ideal port and connecting actual transmission lines cannot be reduced further. We reported in figure 17 the best result allowed by optimization. Unfortunately $|S_{11}|$ reaches its minimum at f_0'=2.438GHz, not exactly at f_0=2.45GHz. Though we obtained such discrepancy, this should not be a problem because this simulation does not represents the real behaviour of the built antenna, whose production is affected by technological limitations related to the quality of the chosen realization process (i.e. leading to fluctuation in the substrate dielectric permittivity, or consistency in line widths and lengths), that eventually leads to difference between simulated and actual antenna. Besides that, the -20dB bandwidth is B_{-20dB}=14.741MHz around f_0'=2.438GHz, whereas B_{-10dB}=49.249MHz, this is a very selective (narrowband) antenna. To sum up, the array looks barely behaving as expected both in- and out-of-band, this must be confirmed by measurements though.

Far field radiation pattern The radiation pattern (with cuts) and the axial ratio are depicted in figures from 21 to 24. These pictures confirm that we have a broadside array (expected, since the radiators are positioned along the x-axis). The ground plane and the beam forming network presence distort the pattern, preventing the array to radiate along negative y-axis tilting the main lobe and directing the maximum radiation along ($\theta = -13°$,$\varphi = 90°$). Moreover, from figure 22 we notice that the antenna is fully linearly polarized at least within the (y,z) plane (since the patch is single-edge fed this is a expected too).

HPBW and SLL From figure 24b,c one has HPBW = 20.4° and SLL=-20.7dB within the (y,z) plane.

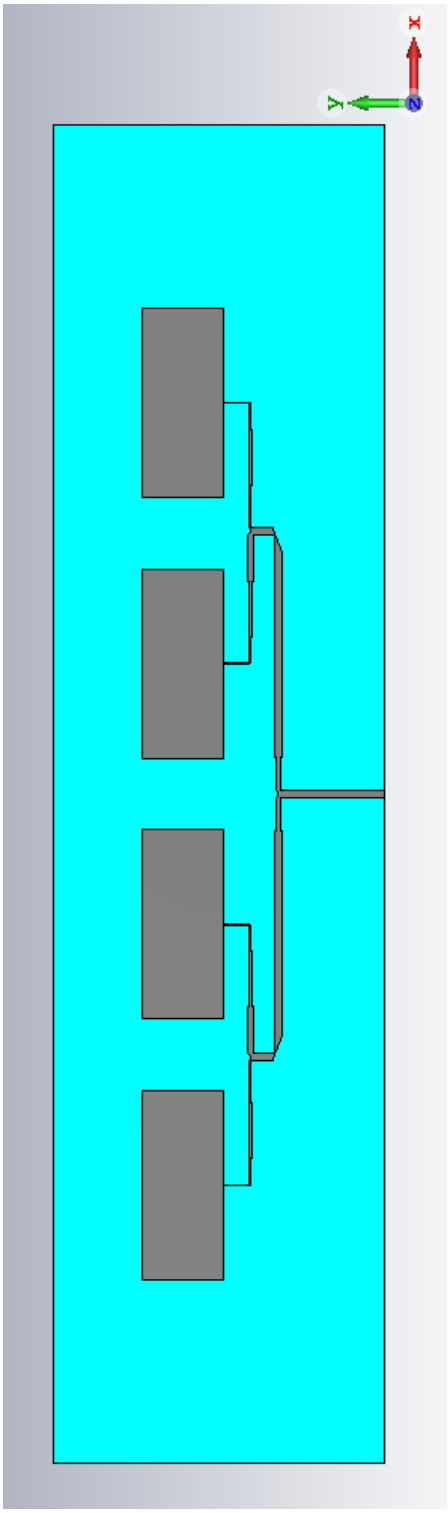

Figure 19: Full array top view, (x,y) plane.

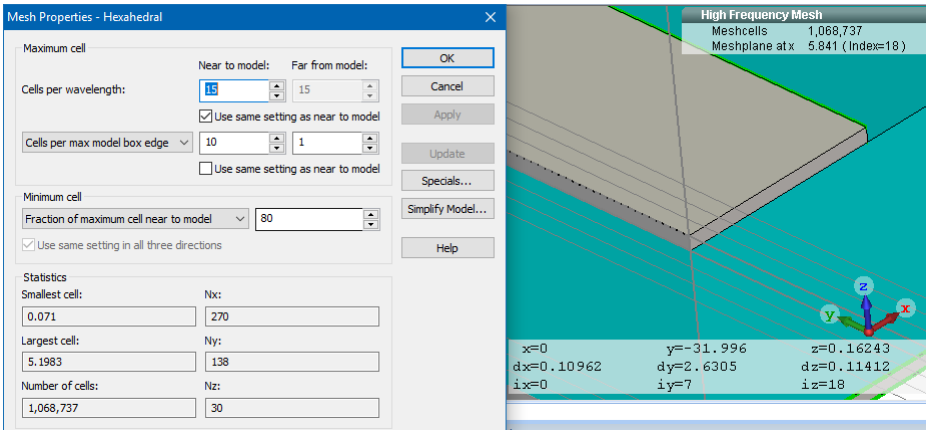

(a) *General settings*

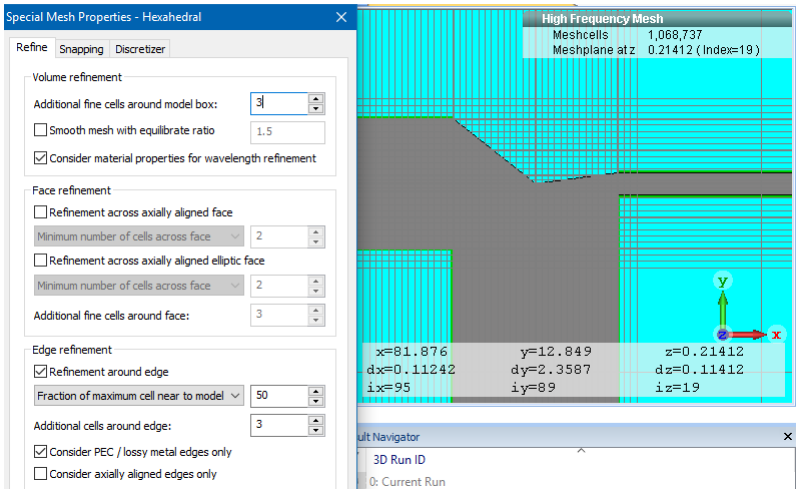

(b) *Special settings*

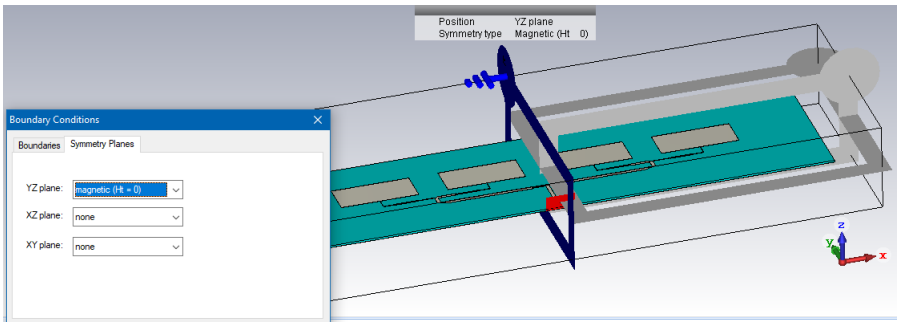

(c) *Boundary conditions: symmetry plane*

Figure 20: Mesh general and special settings. As it appears the mesh has been increased to fit all the bends and narrower lines the best way.

.

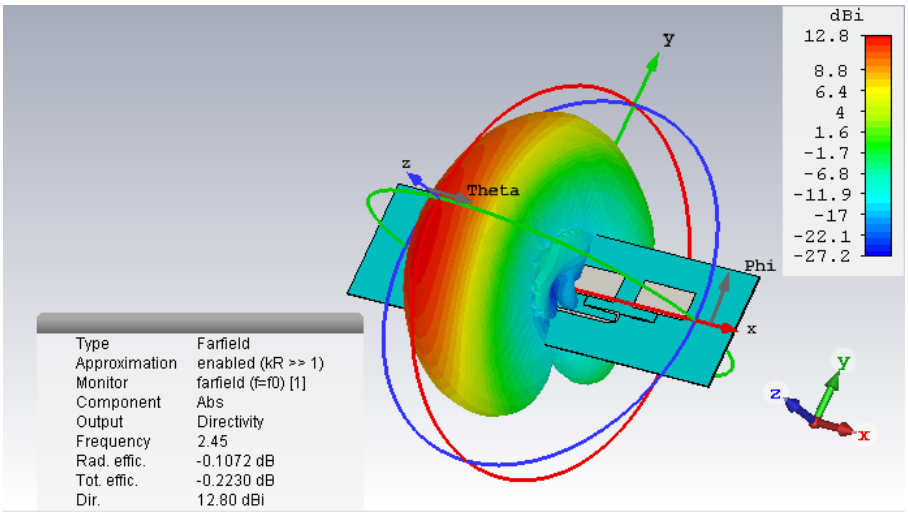

Figure 21: 3D far field radiation pattern.

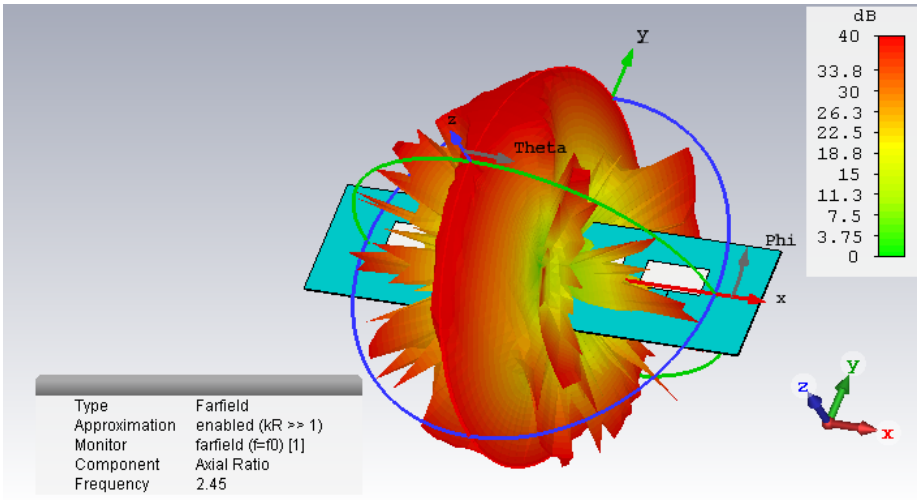

Figure 22: Far field axial ratio.

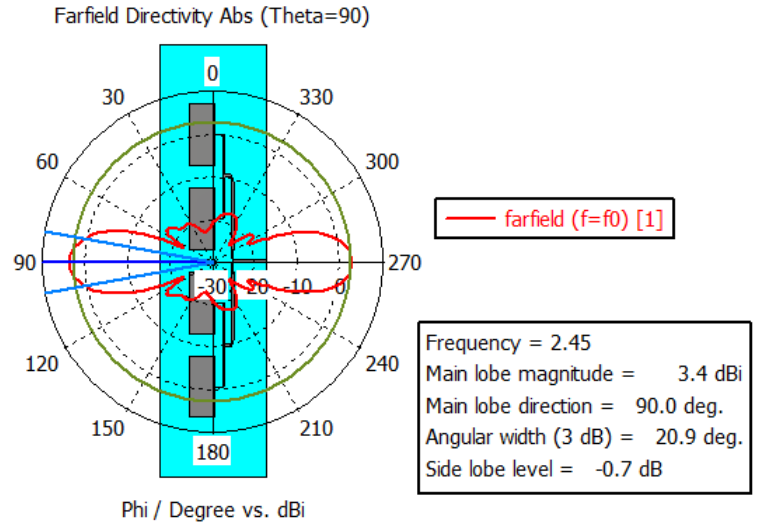

(a) *(x,y) plane cut,* $\theta = 0°$

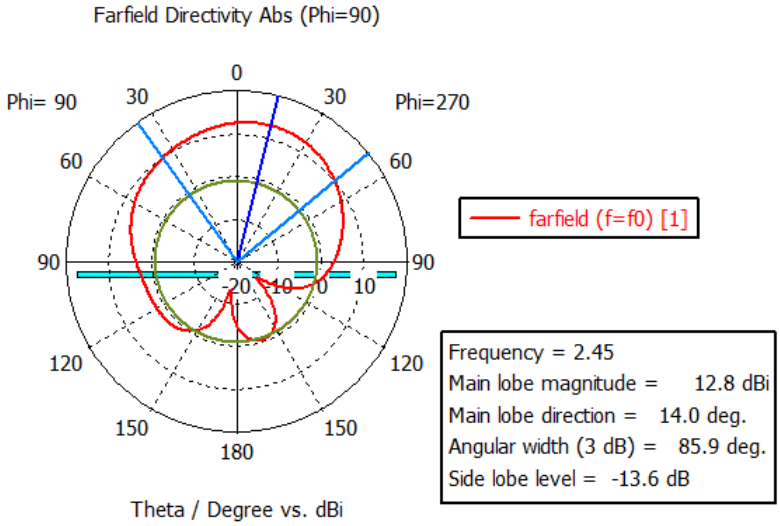

(b) *(y,z) plane cut,* $\varphi = 0°$

Figure 23: Radiation pattern's directivity polar cut planes. As it appears the array radiates broadside within the (y,z) plane. The radiation is minimum along the negative y-direction.

.

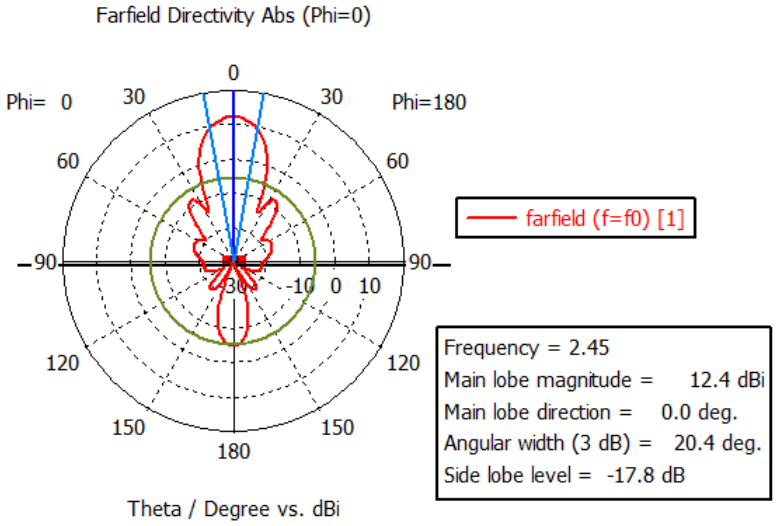

(a) *(x,z) plane polar cut,*$\varphi = 0^\circ$

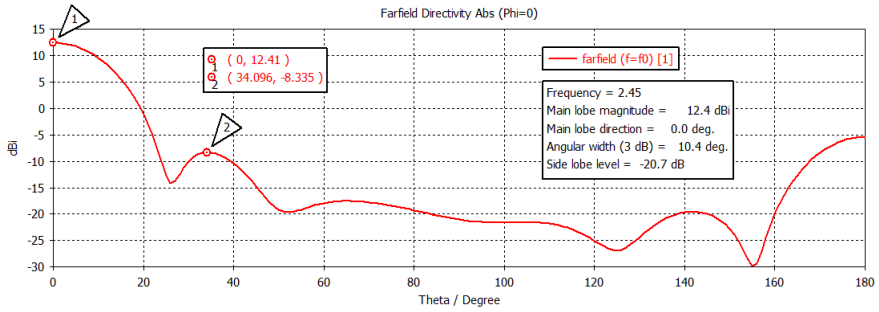

(b) *(x,z) plane cartesian view,* $\varphi = 0^\circ$

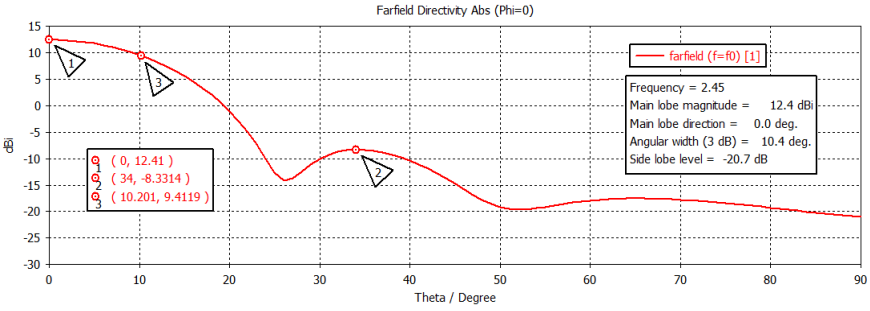

(c) *positive (x,z) plane cartesian view,* $\varphi = 0^\circ$

Figure 24: Radiation pattern's cut planes. As it appears the array radiates broadside within the (y,z) plane. The side lobes level limit is fulfilled, HPBW=20.4°.

.

A Appendix: bends design

Every time a bend is present, it introduces capacitive and inductive contributions to the microstrip line. To compensate this effects we varied the bend angle till the optimum is reached. To design the bend we cut away the highlighted part in figure 25a, obtained by rotating by an angle α a rectangle then subtracted from the bend with boolean transformation. The simulation of the 50Ω bend within the 3dB splitter confirms the compensation (figure 26). Another relevant parameter is represented by the cut's position with respect to the bend's external corner, changed by means of the parameter a that can be found in figure 25b. The input reflection coefficient variation is printed in figure 26.

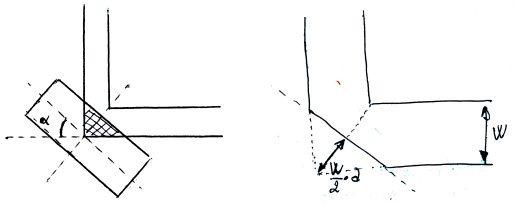

(a) *cut's angle* **(b)** *cut's position*

Figure 25: Bend design

.

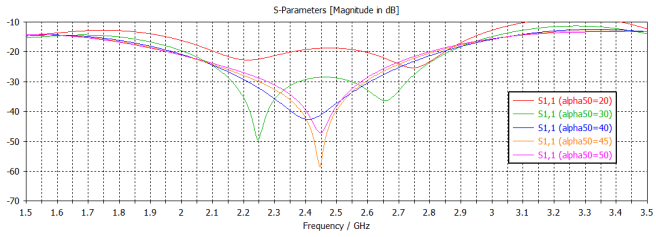

(a) *sweep on* α

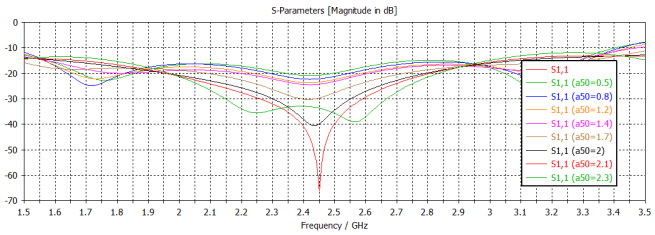

(b) *sweep on a*

Figure 26: Input reflection coefficient varying bend's parameters.

.

B Appendix: mitered T-junction design

Mitered junctions have been used to have better power splitting performance within the BFN. Looking at figure 27b one can notice that the cut is positioned with the aim of giving the power the same path length both toward left and right branch. Referring to figure 27a:

$$l = \sqrt{\left(\frac{W_{50}}{2}\right)^2 + \left(\frac{W_{70}}{2}\right)^2}$$

and

$$\theta = \sin^{-1} \frac{1}{2} \frac{W_{70}}{l}$$

To design the section depicted in figure 27b the same calculations hold.

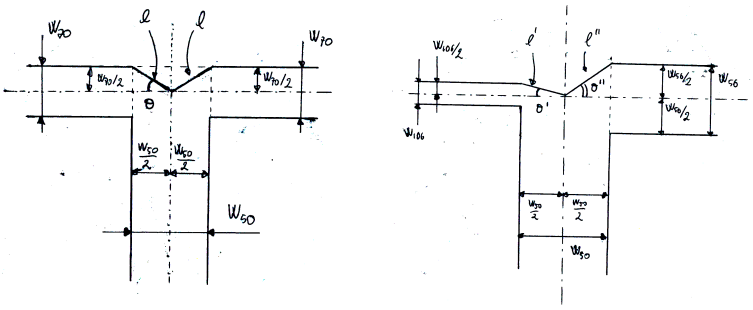

(a) *3dB splitter* **(b)** *5.3dB splitter*

Figure 27: Designed T-junction.

.

C Appendix: input line length dependence

Our 50Ω input line has a length of about 35mm. The connection between the transceiver is likely to happen by means of a coaxial cable, whose length would be actually undefined, then it is important to make the array independent on the input line length. Hence, the BFN must be able both to perfectly match the feeding line with the patches and keep the input reflection coefficient low enough (in our case this is mainly accomplished through the 70Ω quarter wavelength transformers and the 50Ω bends compensation), whichever the feeding line's length.

To verify the good behaviour of the input matching we propose the simulation outcomes depicted in figure 28, where the input vertical 50Ω line length has been changed.

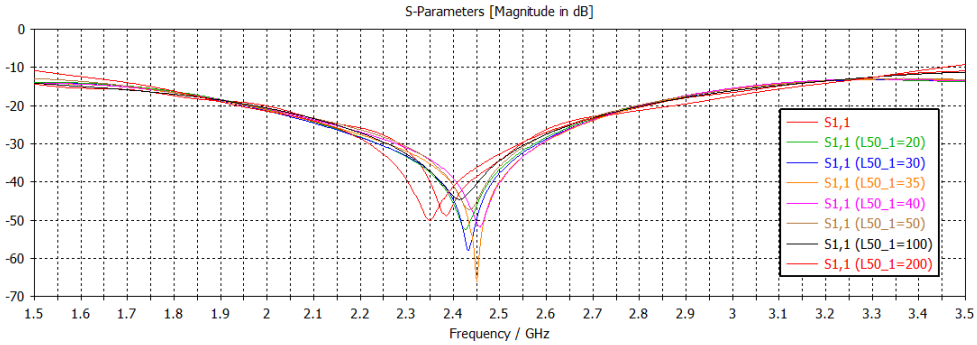

Figure 28: The input line length has been changed, the measures are expressed in millimetres. System is really sensible to lines longer than 50mm, showing a shift in resonance frequency above that value.